

A bioengineered lymphatic vessel model for studying lymphatic endothelial cell-cell junction and barrier function

Aria R. Henderson¹ | Isabelle S. Ilan² | Esak Lee¹

¹Nancy E. and Peter C. Meinig School of Biomedical Engineering, Cornell University, Ithaca, New York, USA

²College of Human Ecology, Cornell University, Ithaca, New York, USA

Correspondence

Esak Lee, Nancy E. and Peter C. Meinig School of Biomedical Engineering, Cornell University, 302 Weill Hall, 237 Tower Rd, 14853 Ithaca, NY, USA.
Email: el767@cornell.edu

Funding information

Cornell Mong Family Fellowship (A.R.H., No grant number available); NSF Graduate Research Fellowships Program (A.R.H., No grant number available); Cornell University Start-up Fund (E.L., A.R.H., No grant number available); Meinig Family Investigator Fund (E.L., A.R.H., No grant number available)

Abstract

Objective: Lymphatic vessels (LVs) maintain fluid homeostasis by draining interstitial fluid. A failure in lymphatic drainage triggers lymphatic diseases such as lymphedema. Since lymphatic drainage is regulated by lymphatic barrier function, developing experimental models that assess lymphatic barrier function is critical for better understanding of lymphatic physiology and disease.

Methods: We built a lymphatic vessel-on-chip (LV-on-chip) by fabricating a microfluidic device that includes a hollow microchannel embedded in three-dimensional (3D) hydrogel. Employing luminal flow in the microchannel, human lymphatic endothelial cells (LECs) seeded in the microchannel formed an engineered LV exhibiting 3D conduit structure.

Results: Lymphatic endothelial cells formed relatively permeable junctions in 3D collagen 1. However, adding fibronectin to the collagen 1 apparently tightened LEC junctions. We tested lymphatic barrier function by introducing dextran into LV lumens. While LECs in collagen 1 showed permeable barriers, LECs in fibronectin/collagen 1 showed reduced permeability, which was reversed by integrin $\alpha 5$ inhibition. Mechanistically, LECs expressed inactivated integrin $\alpha 5$ in collagen 1. However, integrin $\alpha 5$ is activated in fibronectin and enhances barrier function. Integrin $\alpha 5$ activation itself also tightened LEC junctions in the absence of fibronectin.

Conclusions: Lymphatic vessel-on-chip reveals integrin $\alpha 5$ as a regulator of lymphatic barrier function and provides a platform for studying lymphatic barrier function in various conditions.

KEYWORDS

3D bioengineered models, integrin $\alpha 5$, junctions, LV-on-chip, lymphatic barrier function, lymphatic endothelial cells

1 | INTRODUCTION

The lymphatic vascular system, a network of lymphatic vessels (LVs), plays a critical role in human health and disease.^{1–4} LVs maintain

fluid homeostasis in tissues by draining excess interstitial fluid leaked from blood vessels (BVs) and returning the fluid back to the blood circulation.^{5–7} LVs also modulate human adaptive immunity by draining antigen presenting cells and transporting them to lymph

Abbreviations: 2D, two-dimensional; 3D, three-dimensional; BECs, blood endothelial cells; BSA, bovine serum albumin; BVs, blood vessels; Collagen 1, type 1 collagen; EBM-2, endothelial basal media 2; ECM, extracellular matrix; EGM-2MV, endothelial growth media 2 microvascular; HAPLN1, hyaluronan and proteoglycan link protein 1; Integrin $\alpha 5$, integrin alpha 5; JAM-A, junctional adhesion molecule A; LECs, lymphatic endothelial cells; LVs, lymphatic vessels; PDMS, polydimethylsiloxane; Prox-1, prospero homeobox 1; VE-cad, vascular endothelial cadherin.

nodes to activate lymphocytes residing in the lymph nodes.⁸⁻¹⁰ In addition, LVs absorb dietary fat in the intestines¹¹⁻¹³ and remove metabolic wastes in the brain.¹⁴⁻¹⁶ Impaired lymphatic function thus contributes to diverse human diseases, such as lymphedema, immune dysfunction, metabolic diseases, obesity, and neurodegenerative diseases.¹⁶⁻²¹ Furthermore, in cancer, LVs transport tumor cells to the lymph nodes, triggering metastasis.^{22,23} It is also known that tumor LVs induce tumor immune escape and evasion.^{24,25} All of these examples show how the lymphatic vascular system is largely involved and implicated in major human diseases.

Importantly, all of these diseases are linked to lymphatic drainage, a function unique to LVs involving the transport of interstitial fluid, masses like waste solutes, and cells into lymphatic vessels, and distributing them to other parts of a body.^{13,26-29} However, the regulation of lymphatic drainage is incompletely understood. Lymphatic drainage is a well-organized, stepwise phenomenon, which is accomplished by the special anatomy of two distinct LVs with two distinct roles: initial and collecting LVs.³⁰⁻³² The interstitial fluid/masses/cells must be absorbed first by the initial LVs. Thus, the initial LVs have specialized endothelial cell-cell junctions that form permeable cell-cell barriers, so that the initial LVs can easily take up the interstitial fluid/masses/cells.³⁰ Next, the absorbed fluid/masses/cells (termed "lymph") must be transported through the lumen via the collecting LVs to successfully reach the lymph nodes and the subclavian veins to finally enter the blood circulation.^{33,34} To achieve this, collecting lymphatics must be less permeable to minimize the loss of the lymph during the luminal transport.

As mentioned above, lymphatic barrier function or permeability plays a key role in lymphatic drainage processes. Thus, deciphering lymphatic barrier function and its regulation is crucial for understanding physiological lymphatic functions, such as lipid transport, metabolism, and immune regulation,³⁵⁻³⁹ and the pathology of lymphatic diseases.^{4,27,31,40,41} LV barrier function can be influenced by numerous factors, including extracellular matrices (ECM),⁴² endothelial cell-cell junctions,⁴³ endocytosis,⁴⁴ lymph flow,^{45,46} lymphatic smooth muscle cell engagement,²⁸ and interaction with other conditions, such as inflammation.⁴⁷⁻⁴⁹ ECM is one component found to be particularly important in lymphatic junction morphology. Collecting lymphatics have a continuous basement membrane consisting of collagen IV, fibronectin, and laminins, which may be critical for their zipper-like junction morphology,⁵⁰ while lymphatic capillaries have a discontinuous basement membrane containing gaps and consisting of collagen IV, collagen XVIII, nidogen-1, and laminins, which may be critical for their button-like junctions.⁵¹ In addition, lymphatic valve endothelial cells, found in the luminal valves in collecting lymphatics, express high levels of integrin $\alpha 9$, a receptor of fibronectin-E111A/EDA spliced isoform.⁵² ECM components also play a role in lymphatic pathophysiology such as during cancer metastasis via the lymphatic system in which LECs in cancer-associated lymph nodes express the $\alpha 11b$ integrin subunit, leading to fibrinogen adhesion and subsequent LEC contraction to favor tumor intravasation⁵³ or as seen in decreased hyaluronan and proteoglycan link protein 1 (HAPLN1) expression in age-dependent ECM degradation that increases LEC

permeability and impairs both lymph nodes and lymphatic vasculature.⁵⁴ Therefore, isolating and controlling these factors in experimental settings is important to understanding lymphatic function in different contexts. Although animal models have had an impact on discoveries in the field, decoupling the aforementioned elements in animal models is often challenging. Although two-dimensional (2D) *in vitro* models are highly controllable and have provided an *in vitro* platform, they may not recapitulate lymphatic junctions under flow condition in three-dimensional (3D) environments as in *in vivo* settings.⁵⁵ For these reasons, there are strong demands for experimental tools that enable easy control of biological parameters in a more realistic 3D environment.

In this study, we built upon our technologies to create a 3D biomimetic "Lymphatic vessel-on-Chip" (LV-on-chip) model system and use this model to understand lymphatic junctions and barrier function in 3D rudimentary lymphatic structure. The engineered LVs exhibit perfusable lumens and distinct barrier functions under luminal flow and/or different extracellular matrices, which provide an important platform to investigate the process of interstitial fluid/mass transport via LVs or blood vessels (BVs). Using the platform, we reveal integrin $\alpha 5$ as a regulator of lymphatic barrier function.

2 | MATERIALS AND METHODS

2.1 | Cell culture

Primary human dermal microvascular lymphatic endothelial cells (LECs, neonatal) were purchased from Lonza. The cells were isolated from foreskin tissues using CD31 and podoplanin markers. Primary human dermal microvascular blood endothelial cells (BECs, neonatal) were purchased from Lonza. LECs and BECs were cultured in EGM-2MV media (Lonza, Switzerland). These endothelial cells were used in their passages 3-8 and maintained in standard tissue culture incubators at 37°C, 95% humidity, and 5% CO₂. Across all passage numbers (p3-p8), we compared phenotypes both in the culture flasks and in our 3D models. In both situations, we had consistent phenotypes.

2.2 | Microfluidics

Microfluidic devices were fabricated using a soft lithography method as we performed previously.^{56,57} The LV-on-chip device was composed of a cover glass on the bottom and a polydimethylsiloxane (PDMS) gasket on top of the cover glass. PDMS (Sylgard 184, Dow-Corning) was mixed with a curing agent, provided in the Sylgard PDMS kit, at a 10:1 ratio (base:curing agent) and cured overnight at 60°C on a silicon master. The PDMS was removed from the silicon master and surface activated by plasma etching for PDMS bonding to the cover glass. Bonding of the PDMS to the glass was followed by curing at 60°C overnight for permanent bonding. The device was plasma etched for hydrophilic surface modification and treated with 0.01% poly-L-lysine (Sigma, St. Louis, MO) for 1 h, and 1% glutaraldehyde

for 30 min, then rinsed with sterile water 3 times, and further rinsed in sterile water overnight at room temperature. Steel acupuncture needles with a diameter of 0.25 mm were sterilized with 70% ethanol and bovine serum albumin (BSA)-coated, then introduced into the devices. The needle-inserted devices were air-gun dried and UV sterilized for 30 min. Collagen 1 as buffered with phosphate buffered saline (PBS), titrated to a pH of 8.0 with NaOH, giving the final concentration of 2.5 mg/mL (with or without 150 μ g/mL fibronectin) was pipetted into the microfluidic devices and polymerized for 50 min at 37°C. Cell growth medium was then added to the devices overnight and needles were carefully removed to create channels in the collagen 1 gel. After 1 day washing the devices with cell growth medium, LECs or BECs were introduced. LECs or BECs were resuspended at 2×10^6 cells/mL in LEC media, and 100 μ L of cell suspension was introduced into the channel of the device to allow cells to adhere to 3D collagen 1 for 10 min before washing with growth medium. The devices were incubated for 3 days on a rocking platform in the tissue culture incubator, replenishing culture media daily. For determining the shear stress imparted by a rocker, we assumed that the culture medium is a Newtonian fluid in which the viscous stresses arising from its flow, at every point, are linearly correlated to the local strain rate (the rate of change and of its deformation over time). We also assumed that the pressure head driving flow through the channel is gravitational force exerted when the rocker tilts with the angle of 37°. We formulate the following relationship between the angle of the rocker and the wall shear stress (τ)⁵⁸:

$$\tau = r/2 \times \rho \times g \times \sin\alpha$$

where r is the vessel radius, ρ is the fluid density, g is acceleration due to gravity, and α is the angle of the rocker. The rocker tilts the chips from -37° to $+37^\circ$ at a frequency of 2–3 rpm. The diameter of the acupuncture needles is 0.25 mm (the needles are not hollow), which determines vessel radius that is also affected by cell seeding density, collagen swelling, and cell contractility, which creates approximately a shear stress of 3.5–4.5 dyne/cm². This value also falls within the range of 4–12 dyne/cm², which was determined as the *in vivo* value for rat mesenteric prenatal lymphatics.⁵⁹

2.3 | Lymphatic permeability

Lymphatic permeability in microfluidic devices was measured as described previously.^{56,57,60} Briefly, fluorescent dextran (70 kDa, FITC, Life Technologies, Carlsbad, CA) was mixed in the media solution (dextran concentration in the solution: 25 μ g/mL) and 50 μ L of the dextran solution was added to one reservoir that is connected to the other reservoir through the vascular channel. This initial hydrostatic pressure allows fluid to fill the channel. We imaged the vessel area (in 10x field) that is sufficiently far from the dextran injection to minimize data fluctuation due to the initial loading pressure. We imaged dextran for 5 min after injection every 5 s with an SP8 confocal microscope (Leica, Germany), so that we have total 60 consecutive

images per experiment. Regarding the fluorescence measurements, we assumed that the fluorescence intensity is proportional to the number of the molecules in solution and followed that definition to quantify the permeability coefficient, p_d of the vessels,^{58,61} the estimate can be made using the formula:

$$J = P_d (c_{vessel} - c_{ECM}),$$

where $p_d = \left(\frac{2r}{l_0}\right) \left(\frac{\partial I}{\partial t}\right)$, J is the mass flux of the solution, c_{vessel} is the concentration of the fluorescence (Dextran) in the vessel, c_{ECM} is the concentration of the fluorescence in the perivascular extracellular matrix (ECM), r is the vessel radius, and l_0 is the initial intensity of Dextran. By tracing the intensity change $\left(\frac{\partial I}{\partial t}\right)$ in fluorescence in the ECM with the time step of the recording, we could determine the mass flux (the slope of the curve), and calculate the permeability coefficient, p_d . We adopted the automated MATLAB code developed by Polackcheck and colleagues to quantify permeability from time-lapse images.^{56,57,60}

2.4 | Immunostaining and imaging in microfluidics

For immunofluorescent staining and imaging, LECs or BECs embedded in the 3D collagen 1 bulk of the device were fixed with 4% paraformaldehyde for 1 h at room temperature. Fixed devices were permeated with PBST (0.3% Triton-X in PBS) for 45 min at room temperature, then blocked with 3% BSA in PBS overnight at 4°C. Primary antibodies detecting VE-cadherin (Santa Cruz, Dallas, TX, 1:100; or Abcam, UK, 1:100), integrin $\alpha 5$ antibody (clone: SNAKA51) (Sigma, St. Louis, MO, 1:200), JAM-A (Santa Cruz, Dallas, TX, 1:100), CD31 (DAKO, 1:200), Prox-1 (Abcam, UK, 1:100), and CCL21 (MyBioSource, San Diego, CA, 1:100) were incubated in blocking buffer overnight at 4°C. Primary antibodies were washed overnight in PBS at 4°C. Secondary antibodies (all from Invitrogen, Carlsbad, CA, 1:500), Phalloidin (Life Technologies, Carlsbad, CA, 1:200), and DAPI (Sigma, 1:500) were subsequently incubated in blocking buffer overnight at 4°C in dark. The secondary antibodies, phalloidin, and DAPI were washed overnight in PBS at 4°C in dark to remove fluorescent background before confocal microscopy. Confocal images were acquired with an SP8 confocal microscope (Leica, Germany) with a 40x objective. Obtained fluorescent images were z-stacked and adjusted for brightness and contrast using ImageJ.^{62,63} To quantify junctional organization, greyscale micrographs of cells immunostained for VE-cadherin were converted to black and white based on a threshold determined by Otsu's method, and junctional area was defined as the total number of pixels above the threshold.

2.5 | Statistics

Independent two sample populations were compared using unpaired, two-sample *t*-tests with a normal distribution assumption. In statistical analyses with more than two groups, to prevent potential

type 1 errors in the *t*-test, one-way ANOVAs with Tukey's HSD (Honestly Significant Difference) tests were used for group analyses. All data points on graphs represent average values, and error bars depict Standard Error of the Mean (SEM). $p < .05$ was the threshold for statistical significance. *p*-values and sample numbers (*n*) are described in figure legends.

2.6 | Data availability

All relevant data that support the findings and conclusions of this study are available from the corresponding author upon request.

3 | RESULTS

3.1 | Engineered 3D lymphatic and blood vessels show distinct vessel structure and barrier function

To examine lymphatic structure and barrier function, we engineered an organotypic model of lymphatic vessels ('LV-on-chip') building on a previously developed blood vessel-on-chip.^{56,57} Briefly, our PDMS (polydimethylsiloxane)-based LV-on-chip is composed of one hollow cylindrical channel, which is completely embedded into 3D collagen 1 matrix (Figure 1A). In the hollow channel, we seeded human dermal microvascular lymphatic endothelial cells (LECs) to form a biomimetic lymphatic vessel (Figure 1A). This biomimetic LV was positive for CCL21, indicating that the model has characteristics of lymphatic capillary (Figure S1). The EGM-2MV media was introduced to circular reservoirs (inlet and outlet) that are directly connected to the lymphatic endothelial channel. Luminal shear flow of 3.5–4.5 dyne/cm² was initiated to culture the LECs by rocking the LV-on-chip device in a tissue culture incubator. After 3 days of culture, the device was fixed and LECs were stained with anti-human Prox-1 (green) and anti-human CD31 (red) antibodies to assess lymphatic endothelial identity and cell morphology (Figure 1A). We next compared human dermal microvascular blood endothelial cells (BECs) with LECs in the same platform to investigate distinct vessel structure and function (Figure 1B). After 1 day of cell seeding and culture under luminal flow, we observed that BECs became more contractile than LECs, forming engineered blood vessels (BVs) with smaller vessel diameters compared to LECs (Figure 1B). BECs showed 66.7 ~ 68.2% decreases in lumen size while LECs only showed 21.3 ~ 23.5% decreases in lumen size. This was consistent with our observation of BVs and LVs in mouse ears *in vivo* (Figure 1C) and therefore supports the validity of the vessel morphology in our biomimetic model. Next, we fixed the devices and stained the cells with phalloidin and anti-VE-cad (VE-cadherin) antibody to visualize F-actin and endothelial adherens junctions (Figure 1D). F-actin was localized in cell peripheries around the junctional areas in engineered BVs (BEC), whereas in the cytoplasmic areas in engineered LVs (LEC). VE-cad was mostly found in the junctional areas in engineered BVs, forming tighter adherens junctions, whereas diffused,

cytoplasmic distribution of VE-cad in LVs formed the weaker or loosened adherens junctions (Figure 1D).

To assess lymphatic and blood vessel barrier function, we cultured BV/LV-on-chip for 3 days on the rocking platform, providing same degree of shear stress, and introduced 70 kDa dextran into the vessel lumens and observed dextran diffusion in real time under microscopy (Figure 1E). Engineered BVs kept dextran from leaking out of the vessels; however, engineered LVs were more permeable than BVs, which was enough for dextran to quickly escape the vessels and diffuse to the interstitium (Figure 1E). Furthermore, our quantitative analysis of dextran leakage indicated that engineered LVs are 3.44 times more permeable than BVs with a *p*-value of .0016 (*n* = 5) (Figure 1F). This suggests that LECs and BECs form very different cell-cell junctions under luminal flow, exhibiting significantly different permeability or barrier function in our biomimetic vessel-on-chip model. Taken together, the engineered 3D lymphatic and blood vessels showed distinct vessel junction morphologies and levels of barrier function.

3.2 | Fibronectin appears to tighten lymphatic junctions

We next focused on engineered LVs and studied how lymphatic cell-cell junctions are regulated by the extracellular matrix (ECM) (Figure 2). To quickly screen ECM effects, we cast different types of ECM hydrogels into well plates in 2D. We used 2.5 mg/mL collagen 1, which is the same condition we had in the LV-on-chip experiments in Figure 1. We also used mixture of 2.5 mg/mL collagen 1 and 150 µg/mL fibronectin from stock solutions of a defined concentration. As controls, we also tested plastic dishes without ECM hydrogel (Figure 2A). After 1 day of culture, we fixed the cells and stained them with phalloidin and anti-VE-cad antibodies. On the plastic dish, in relatively stiffer condition with a Young's modulus of 2.28–3.28 GPa⁶⁴ compared to the Young's modulus of collagen 1 at only 0.5–12 kPa,⁶⁵ LECs appeared to have very tightened junctions. F-actin and VE-cad were strongly localized in the junctional area (Figure 2A, top). On the 2D collagen 1 hydrogel, LECs showed apparently much more diffuse junctions, which was consistent with the phenotype that we observed in our LV-on-chip. F-actin was in cytoplasm and junctional localization of the VE-cad was weaker than LECs on plastic dish. We also found gaps between cells (Figure 2A, middle). On the 2D collagen 1 + fibronectin hydrogel, LECs showed more tightened junctions than LECs in collagen 1 (Figure 2A, bottom). F-actin and VE-cad were localized in the junctional area, compared to those in LECs in collagen 1, which was more similar to the phenotype of engineered BVs on-chip in Figure 1. We also saw differences in LEC morphology between groups with the LECs cultured on stiff plastic appearing more elliptical and having a defined axis of alignment while the LECs grown on collagen 1 + fibronectin had a rounder, more cobblestone appearance. One-way ANOVA with Tukey's HSD test-based quantification of the relative junction area illustrated a decrease in junction area between the cells grown on plastic and

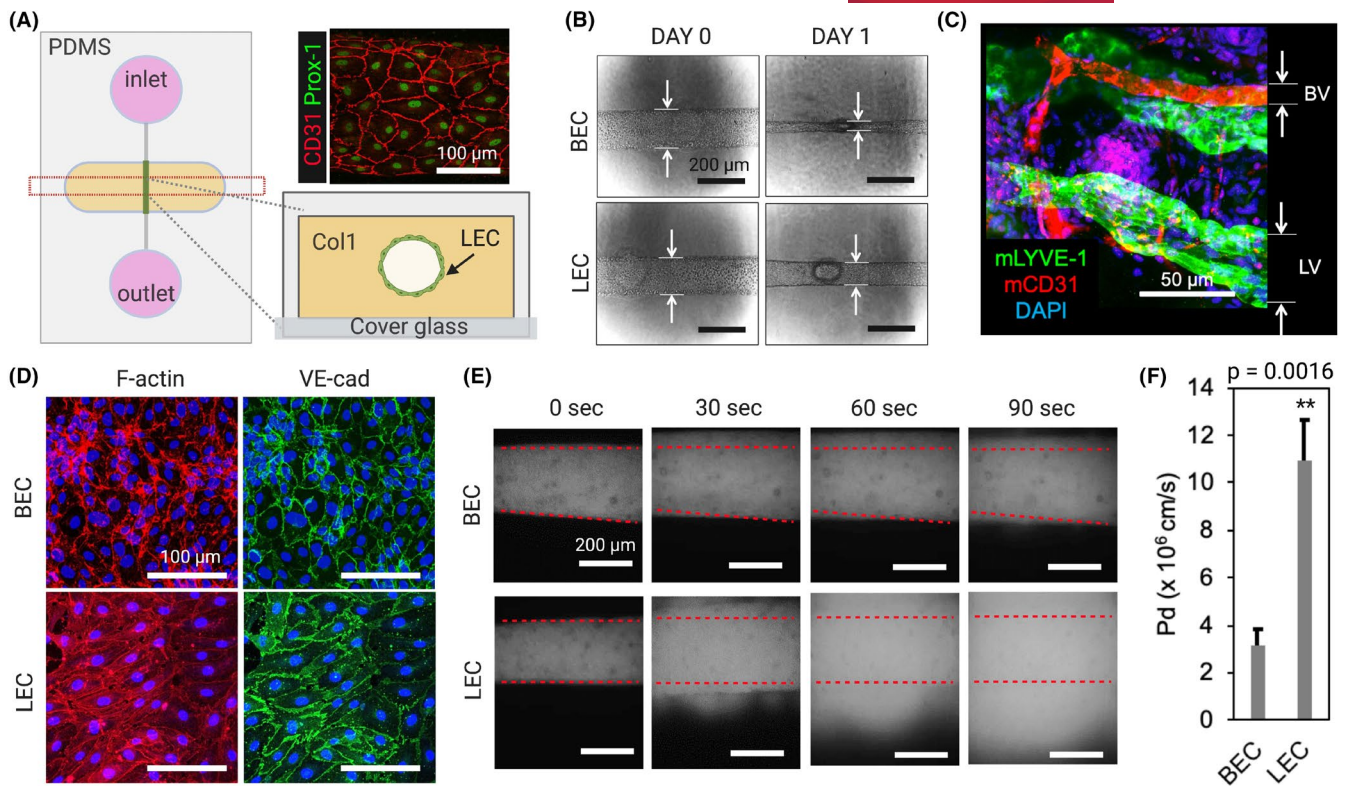


FIGURE 1 Engineered 3D lymphatic and blood vessels show distinct vessel structure and barrier function. (A) A schematic of an organotypic 3D lymphatic vessel model (LV-on-chip). Prox-1 (green) and CD31 (red) expression confirms lymphatic endothelial identity and cell morphology in the channel. (B) Morphologic changes in human dermal microvascular blood endothelial cells (BECs) with lymphatic endothelial cells (LECs) after 1 day of cell seeding. BECs become more contractile than LECs, forming a smaller vessel diameter compared to LECs. (C) BVs and LVs observed in mouse ear tissues. mLYVE-1, anti-mouse LYVE-1 antibody; mCD31, anti-mouse CD31 antibody. (D) Phalloidin (red) and anti-VE-cad (VE-cadherin) antibody (green) staining to visualize F-actin and adherens junctions. (E) Lymphatic and blood vessel barrier function. 70 kDa dextran was introduced into the vessel lumens and dextran diffusion was observed in real time under microscopy. Superimposed red dashed lines represent the edges of the vessel lumens. (F) Quantification of the permeability of BEC-generated engineered BVs and LEC-generated LVs. $**p = .0016$, two-tailed unpaired Student *t*-test, $n = 5$ per group. Data are expressed as mean \pm S.E.M

the cells grown on collagen 1 gel ($**p = .0017$, $n = 6$); no significant difference between the cells cultured on collagen 1 + fibronectin compared to the cells grown on plastic ($p = .5292$, $n = 6$); an increase in junction area between the cells grown on collagen 1 and the cells grown on collagen 1 + fibronectin ($*p = .0151$, $n = 6$). (Figure 2B). We next sought to understand the dynamics of fibronectin on these two different culture conditions by sparsely seeding LECs at 10% confluence on collagen 1 or collagen 1 + fibronectin gel (Figure 2C). After 1 day of culture, we fixed the cells and stained them with anti-VE-cad and anti-fibronectin antibodies. On collagen 1 gel, we saw LEC islands with VE-cad expression but a lack of fibronectin expression (Figure 2C, top). On collagen 1+ fibronectin, we saw LEC islands with VE-cad and fibronectin. Interestingly, we often observed fibronectin connecting separate LEC islands like cloth patches stitched with sewing thread (Figure 2C, middle and bottom). We next cultured these cells for a longer period of time, and at day 4, traced fibronectin and adherens junctions. LECs showed apparently tightened junctions as we expected in collagen 1 + fibronectin condition (Figure 2D). Interestingly, fibronectin was also localized in the junctional area (Figure 2D). Taken together, fibronectin appeared to

connect LEC islands, like stitches, and is localized in the junctional area of the tightened LEC monolayer on the collagen 1 + fibronectin gel.

3.3 | Fibronectin-Integrin $\alpha 5$ axis regulates lymphatic junctions and barrier function

Based on the 2D gel-based experiments described in Figure 2, we moved onto our 3D LV-on-chip system to assess the role of fibronectin in 3D culture and to determine fibronectin effects on lymphatic junctions and barrier function (Figure 3). We prepared LV-on-chip composed of one hollow channel, which is embedded into 3D collagen 1 or collagen 1 + fibronectin matrix (Figure 3A). In the hollow channel, we seeded LECs and the cells were cultured in the devices on a rocking platform for 3 days. We then fixed the devices and stained the cells with anti-VE-cad (VE-cadherin) and anti-JAM-A (junctional adhesion molecule A) antibody to visualize endothelial adherens junctions and tight junctions (Figure 3A). VE-cad staining showed modest changes in adherens junctions from

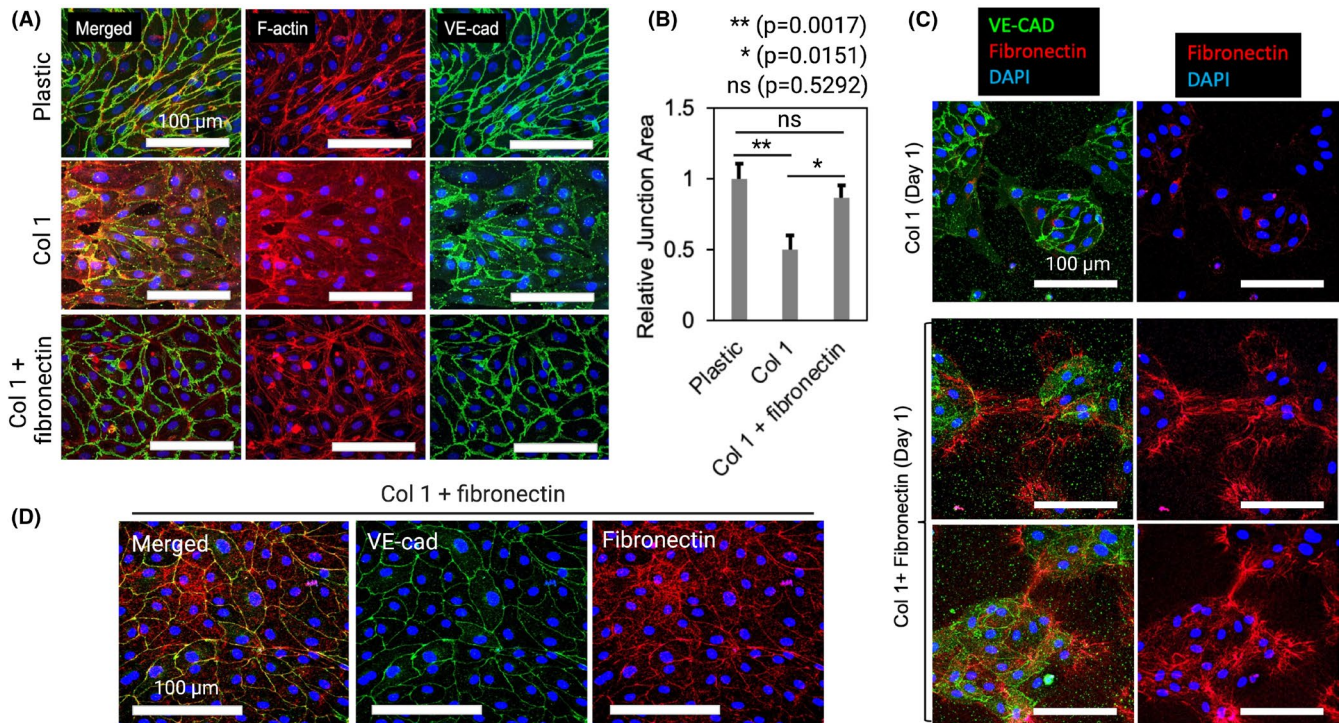


FIGURE 2 Fibronectin tightens lymphatic junctions. (A) Lymphatic endothelial cells (LECs) in different ECM hydrogels (2D): 2.5 mg/mL collagen 1, 2.5 mg/mL collagen 1 and 150 μ g/mL Fibronectin, and no gel (plastic). F-actin and VE-cad were visualized to assess cytoskeletal arrangement and adherens junction formation in each condition. (B) Quantification of the relative junction area was performed, illustrating a significantly lower junction area in cells grown on the 2.5 mg/mL collagen 1 compared to the cells grown directly on plastic. ** $p = .0017$ (Collagen 1 vs. plastic); higher junction area in cells grown on the 2.5 mg/mL collagen 1 + fibronectin compared to the cells grown on collagen 1. * $p = .0151$ (Collagen 1 + fibronectin vs. Collagen 1); not-significant (ns) $p = .5292$ (Collagen 1 + fibronectin vs. plastic). One-way ANOVA with Tukey's HSD tests, $n = 6$ per group. Data are expressed as mean \pm S.E.M. (C) Dynamics of fibronectin on LECs in collagen 1 or collagen 1 + fibronectin gel. On collagen 1 gel, LEC islands with VE-cad expression lacks fibronectin expression. On collagen 1 + fibronectin, fibronectin connects separate LEC islands. (D) At day 4 on Collagen 1 + fibronectin, LECs showed tightened junctions and fibronectin was localized in the junctional area

the jagged, weaker adherens junctions in collagen 1 to apparently more tightened junctions in collagen 1 + fibronectin (Figure 3A, top). Staining with antibodies for a tight junction marker JAM-A showed more dramatic changes (Figure 3A, bottom). In the collagen 1 condition, JAM-A was so diffusive in LEC cytoplasm that it was difficult to tell where cell-cell junctions existed under microscopy (Figure 3A, bottom left). Strikingly, adding fibronectin in the collagen 1 gel strongly tightened tight junctions in LECs (Figure 3A, bottom right). We also saw an apparent change in cell morphology with the cells in the combination collagen 1 + fibronectin matrix exhibiting less alignment and more of a cobblestone shape than either the plastic control condition or the pure collagen 1 condition, similar to the changes seen in the 2D experiment above. We next performed a loss of function experiment by using anti-integrin $\alpha 5$ neutralizing antibodies, since fibronectin signaling is primarily mediated via integrin $\alpha 5$.^{66,67} In the collagen 1 + fibronectin condition, we compared anti-integrin $\alpha 5$ antibodies and the vehicle conditions by treating 50 μ g/mL of antibodies or vehicles at day 2 and performed our staining at day 3. The integrin $\alpha 5$ blockade appeared to reverse tightened junctions in the collagen 1 + fibronectin condition (Figure 3B). One-way ANOVA with Tukey's HSD

test-based quantification of the junction area showed a higher junction area in the collagen + fibronectin condition compared to either the collagen 1 condition (** $p = .0041$, $n = 6$) or the collagen 1 + fibronectin + integrin $\alpha 5$ antibodies condition (** $p = .0010$, $n = 6$) (Figure 3C).

To assess lymphatic vessel barrier function in each condition, we cultured LV-on-chip for 3 days either in collagen 1 or collagen 1 + fibronectin, on the rocking platform, providing the same degree of shear stress. Then, we treated 50 μ g/mL of anti-integrin $\alpha 5$ antibodies or vehicles and cultured them for one additional day on the rocking platform. On day 3, we introduced 70 kDa of dextran into the vessel lumens and observed dextran diffusion in real time under microscopy (Figure 3D). Engineered LVs in collagen 1 showed the leaky barrier (the more permeable barrier), but LVs in collagen 1 + fibronectin showed a much-enhanced lymphatic barrier (low permeability), whereas the additional anti-integrin $\alpha 5$ antibody treatment to the LVs in collagen 1 + fibronectin made the barrier more permeable (Figure 3D). Moreover, our quantitative analysis of dextran leakage showed that fibronectin significantly reduced permeability in LECs (** $p = .0017$, $n = 5$) and anti-integrin $\alpha 5$ antibody treatment abolished the fibronectin effect (* $p = .0114$, $n = 5$), reversing the

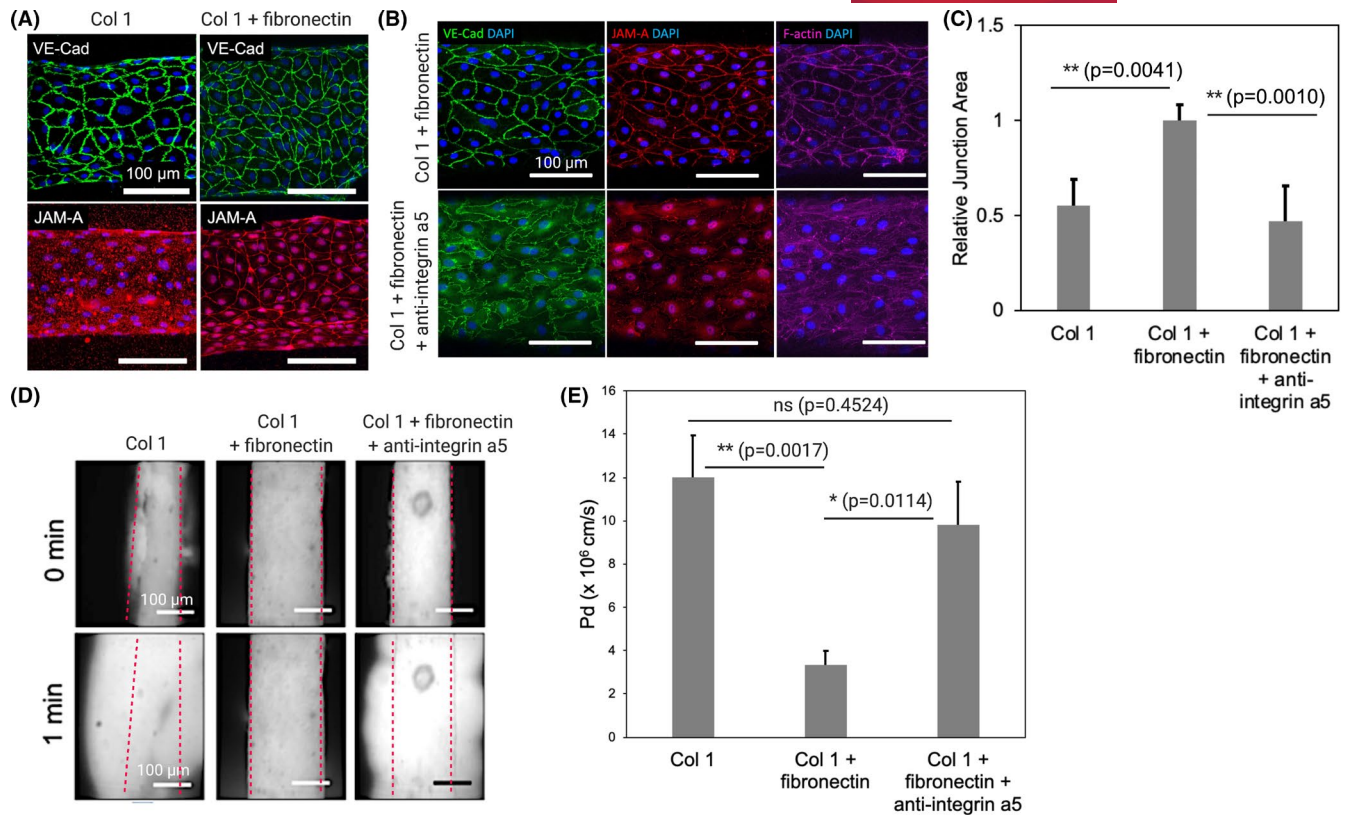


FIGURE 3 Fibronectin-Integrin $\alpha 5$ axis regulates lymphatic junctions and barrier function. (A) VE-cadherin (VE-cad) and junctional adhesion molecule A (JAM-A) staining to visualize adherens junctions and tight junctions in LV-on-chip embedded in Collagen 1 or Collagen 1 + fibronectin matrix. (B) A loss of function experiment by using anti-integrin $\alpha 5$ neutralizing antibodies. In the Collagen 1 + fibronectin condition, 50 $\mu\text{g}/\text{mL}$ of anti-integrin $\alpha 5$ antibodies or the vehicle were treated, and VE-cad, JAM-A, and F-actin were visualized. (C) Quantification of the relative junction area was performed, illustrating a significantly higher junction area in cells grown in the Collagen 1 + fibronectin condition compared to the cells grown in either the Collagen 1 or Collagen 1 + fibronectin + integrin $\alpha 5$ antibodies conditions. $**p = .0041$ (Collagen 1 + fibronectin vs. Collagen 1); $**p = .0010$ (Collagen 1 + fibronectin vs. Collagen 1 + fibronectin + integrin $\alpha 5$ antibodies); one-way ANOVA with Tukey's HSD tests, $n = 6$ per group. Data are expressed as mean \pm S.E.M. (D) Lymphatic vessel barrier function. 70 kDa dextran were perfused into the vessel lumens and dextran diffusion was observed in real time under microscopy. Superimposed red dashed lines represent the edges of the vessel lumens. (E) Quantification of the permeability of LEC-generated engineered LVs in different ECM and antibody treatment conditions. $**p = .0017$ (Collagen 1 vs. Collagen 1 + fibronectin); $*p = .0114$ (Collagen 1 + fibronectin vs. Collagen 1 + fibronectin + integrin $\alpha 5$ antibodies); not-significant (ns) $p = .4524$ (Collagen 1 vs. Collagen 1 + fibronectin + integrin $\alpha 5$ antibodies). One-way ANOVA with Tukey's HSD tests, $n = 5$ per group. Data are expressed as mean \pm S.E.M

permeability to the level of that in LECs in collagen 1 (ns, not significant, $p = .4524$, $n = 5$) (Figure 3E). These data demonstrate that fibronectin-integrin $\alpha 5$ axis regulates lymphatic junctions and lymphatic barrier function.

3.4 | Integrin $\alpha 5$ activation tightens lymphatic junctions

Next, we sought to understand the role of integrin $\alpha 5$ activation in lymphatic barrier function using the LV-on-chip system (Figure 4) since we observed apparently tightened LEC junctions culture conditions with fibronectin addition to collagen 1 (Figures 2 and 3). We hypothesized that fibronectin addition will activate integrin $\alpha 5$ in LECs. To test this hypothesis, we visualized activated integrin $\alpha 5$ by using anti-integrin $\alpha 5$ antibodies (clone: SNAKA51) that can only

detect the activated form of the integrin $\alpha 5$ (Figure 4A). Interestingly, LECs in collagen 1 expressed integrin $\alpha 5$, but this integrin $\alpha 5$ was maintained as an inactivated form, which was not detected by anti-integrin $\alpha 5$ antibodies (clone: SNAKA51). As expected, diffused F-actin with permeable junctions was observed in this condition (Figure 4A, left). However, integrin $\alpha 5$ is activated in fibronectin. Lastly, we examined the role of integrin $\alpha 5$ activation in LECs cultured in collagen 1 without fibronectin. We hypothesized that integrin $\alpha 5$ activation itself can tighten LEC junctions. To test this hypothesis, we treated LECs in collagen 1 with anti-integrin $\alpha 5$ antibodies (clone: SNAKA51), which can activate integrin $\alpha 5$. After overnight treatment, we then fixed the samples and stained with anti-VE-cadherin, anti-JAM-A, and anti-F-actin antibodies. We showed that integrin $\alpha 5$ activation in LECs cultured in collagen 1 tightened LEC junctions without adding fibronectin (Figure 4B). Unpaired, two-sample t-test-based quantification of the junction area confirmed this apparent

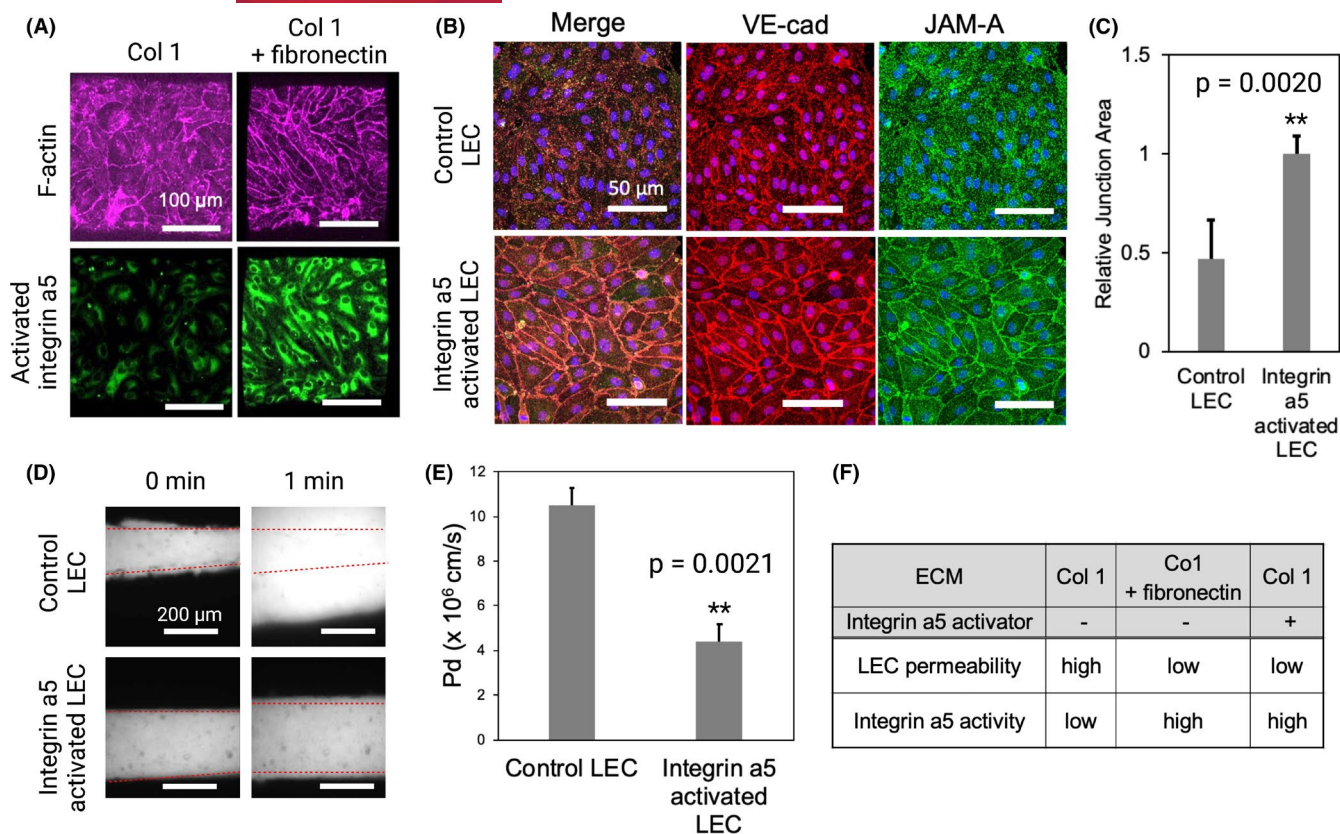


FIGURE 4 Activated integrin $\alpha 5$ tightens lymphatic junctions. (A) Activated integrin $\alpha 5$ was visualized in both ECM composition conditions by using anti-integrin $\alpha 5$ antibody (clone: SNAKA51) that can only detect the activated form of the integrin $\alpha 5$. F-actin was also observed in these conditions. (B) LECs in Collagen 1 were pre-treated with anti-integrin $\alpha 5$ antibodies (clone: SNAKA51) antibodies to activate integrin $\alpha 5$ in LECs. The fixed samples were stained with anti-VE-cadherin antibodies, anti-JAM-A antibodies, and phalloidin to visualize adherens junctions and F-actin. (C) Quantification of the relative junction area was performed, illustrating a significantly higher junction area in integrin $\alpha 5$ -activated cells compared to the control LECs. $**p = .0020$; Two tailed unpaired Student *t*-test, $n = 6$ per group. Data are expressed as mean \pm S.E.M. (D) Control LECs or LECs with activated integrin $\alpha 5$ were seeded in LV-on-chip and cultured for 3 days on the rocking platform. 70 kDa dextran was introduced to the lymphatic lumens. Dextran diffusion was observed at 0 and 1 min under microscopy. Superimposed red dashed lines represent the edges of the vessel lumens. (E) Quantification of the permeability of LEC-generated engineered LVs in collagen 1 with and without integrin $\alpha 5$ activation. $**p = .0021$. Two tailed unpaired Student *t*-test, $n = 5$ per group. Data are expressed as mean \pm S.E.M. (F) This table summarizes our findings regarding LEC permeability and integrin $\alpha 5$ activity. LVs grown in Collagen 1 without any activator treatment showed high LEC permeability and low integrin $\alpha 5$ activity. In contrast, LVs grown in either Collagen 1 + Fibronectin or LVs grown in only Collagen 1 with integrin $\alpha 5$ activator pre-treatment both showed low LEC permeability and high integrin $\alpha 5$ activity

increase in junction area between control LECs and integrin $\alpha 5$ -activated LECs ($**p = .0020$, $n = 6$) (Figure 4C). We then once again performed a fluorescent dextran experiment with real-time imaging to assess the barrier function in LECs in collagen 1 with and without integrin $\alpha 5$ activation (Figure 4D). These data were quantified and showed a decrease in permeability and increase in barrier function following integrin $\alpha 5$ activation (Figure 4E), similar to the changes seen in LECs cultured in collagen 1 + fibronectin (Figure 3D,E). The chart in Figure 4F summarizes our permeability results across the experiments of LVs in collagen 1, LVs in collagen 1 + fibronectin, and LVs in collagen 1 with the integrin $\alpha 5$ activator. In both the collagen 1 + fibronectin condition and the collagen 1 with integrin $\alpha 5$ activator condition, integrin $\alpha 5$ was activated, permeability was decreased, barrier function was increased, and junctions appeared to be tightened.

4 | DISCUSSION

In this study, we developed an *in vitro* 3D engineered lymphatic vessel (LV)-on-chip platform using soft lithography and studied LV junction morphogenesis and barrier function under luminal flow condition (Figure 1). Since lymphatic endothelial cells (LECs) in lymphatic capillaries have weaker barrier function, compared to blood endothelial cells (BECs in blood capillaries), our study more focused on understanding how originally permeable LEC barriers could be regulated by different extracellular matrix (ECM) or directly by adhesion receptor activation. We assessed LV permeability by introducing fluorescently labeled dextran into the vascular lumens of the 3D engineered LV that is embedded in collagen 1. From this study, we found that lymphatic barrier function is increased by adding fibronectin to the collagen 1 ECM, which can be subsequently

reversed by integrin $\alpha 5$ inhibition (Figures 2 and 3). We further discovered that LECs in collagen 1 express inactivated integrin $\alpha 5$ while LECs in collagen 1 + fibronectin ECM express activated integrin $\alpha 5$ and enhance barrier function (Figure 4), demonstrating that integrin $\alpha 5$ activity regulates lymphatic junctions and barrier function. Many chemical stimuli (for example, TNF- α , VEGF-C, and thrombin) have previously been discovered to affect lymphatic barrier function via pathways such as ROCK and cAMP.⁴ Our work adds to this collection by identifying integrin $\alpha 5$ activation as a mediator of lymphatic permeability. The role of fibronectin in vascular function is still being elucidated. In neonatal murine blood vessels, fibronectin regulates angiogenesis in the retina via $\alpha 5$ and αv integrins.⁶⁸ Fibronectin is also understood to be deposited by pericytes, so it may play a role in ectopic pericyte coverage mediated lymphedema. Future studies will focus on determining the role fibronectin plays in lymphatic dysfunction.

Our study focused on our 3D biomimetic *in vitro* model with supporting 2D *in vitro* data rather than *in vivo* models. *In vitro* models are best suited for studying complex microphysiology that might not be easily studied in traditional *in vivo* models,⁶⁹ our manipulation of the ECM by adding fibronectin. Our model also enabled us to independently control luminal flow and monitor vascular permeability, which is often more difficult in *in vivo* models. Furthermore, by using an *in vitro* model, we work directly with primary human endothelial cells and ensure that our integrin $\alpha 5$ findings are relevant to human physiology. Indeed, animal models often do not adequately predict the clinical efficacy of novel therapeutics or mechanisms in human trials due to inter-specific genetic variation.⁷⁰⁻⁷² Since 3D *in vitro* models also can recapitulate the structure and morphology of lymphatic vessels compared to the flat 2D culture on plastic *in vitro* models, there has been development of 3D *in vitro* lymphatic vessel models that are tailored to specific purposes. While our model focuses on cell to ECM interactions and barrier functions, other groups focus on recapitulating other aspects of microphysiology or exploring how certain disease states affect LVs. Some examples include *in vitro* models that are used to investigate solute changes in the lymphatic system,^{44,73} mechanical loading and remodeling,⁷⁴ lymphangiogenesis,⁷⁵⁻⁷⁷ and lymphatic interaction with tumor microenvironments.⁷⁸ Other models have also been developed for monitoring lymphatic drainage with collagen 1 scaffolds to investigate drainage beyond the vessel.^{79,80}

Lymphatic barrier function is largely determined by the type of junction found in the lymphatic vessel. Initial lymphatic vessels have discontinuous button junctions, and these junctions allow the transport of paracellular fluid into the lymphatic lumen *in vivo*.⁴ These lymphatic junctions result from the leaflet shape of the LECs and accompanying adherens junction protein (such as VE-cadherin) expression patterns.³⁰ Healthy lymphatic permeability allows the intravasation and subsequent transport of lipids, immune cells, and solutes in the paracellular fluid while lymphatic permeability dysfunction can result in chronic diseases such as lymphedema. In our experiments, we saw BECs' permeability ($3.0 \sim 4.0 \times 10^{-6}$ cm/s), LECs' permeability ($10.0\text{--}11.0 \times 10^{-6}$ cm/s).

Previously, solute permeability (P_s) in collecting lymphatic vessels was found to be $2.5 \sim 6 \times 10^{-7}$ cm/s by Scallan & colleagues using their *in vivo* model.⁸¹ A different paper from Scallan & colleagues found that the P_s for lymphatic capillaries was 14×10^{-7} cm/s.⁸² A study from Price & colleagues, the barrier function of engineered LEC tubes was determined with the permeability coefficients to bovine serum albumin and 10 kDa dextran of 1.4×10^{-6} cm/s and 1.7×10^{-6} cm/s, respectively.⁸³ These illustrate that lymphatic capillaries have a higher permeability value than collecting lymphatics *in vivo*, and that our and other's engineered lymphatic vessels were much more permeable than the *in vivo* lymphatic vessels. This might be because the *in vitro* models did not carry mural cells (smooth muscle cells) or stromal cells (fibroblasts) in their models and the lumen size is relatively bigger than that in the native lymphatics. Also, our model had a rocker-based oscillatory flow condition for BECs and LEC which was not ideal for those vessels and could be considered a limitation. Better *in vitro* models mimicking native vessel structure, size, multicellularity, and flow remain to be further explored.

In this study, we used a 3D model to demonstrate that lymphatic barrier function is regulated by the activation of integrin $\alpha 5$. Our simple model of lymphatic vessels provided sufficient complexity to reveal the lymphatic junction morphogenesis, yet allowed us to introduce a specific ECM and direct integrin $\alpha 5$ activation to isolate signaling pathways involved in the process. Going forward, inclusion of lymphatic mural cells, immune cells, cancer cells, various ECM components (e.g., lymphatic valve-related, anchoring filament related proteins) or more flow patterns (e.g., interstitial, luminal, unidirectional, oscillatory) could be introduced in this engineered 3D model to more faithfully study the roles of lymphatic barrier function in fluid homeostasis, host immunity, and cancer.

5 | PERSPECTIVES

1. Activated integrin $\alpha 5$ enhances lymphatic barrier function.
2. LV-on-chip provide a platform to investigate biological factors that contribute to lymphatic barrier function.

ACKNOWLEDGEMENTS

A.R.H., I.S.I., and E.L. are supported by the Cornell University Start-up funds, and the Nancy and Peter Meinig Family Investigator funds. A.R.H. is supported by the Cornell Mong Family Fellowship and NSF Graduate Research Fellowships Program (NSF GRFP). This work was performed in part at the Cornell NanoScale Facility (CNF), a member of the National Nanotechnology Coordinated Infrastructure (NNCI), which is supported by the National Science Foundation (Grant NNCI-1542081).

DATA AVAILABILITY STATEMENT

Data are available in the main text or the supplementary materials. Additional data that support the findings of this study are available from the corresponding author upon reasonable request.

REFERENCES

1. Kesler CT, Liao S, Munn LL, Padera TP. Lymphatic vessels in health and disease. *Wiley Interdiscip Rev Syst Biol Med*. 2013;5(1):111-124.
2. Jurisic G, Detmar M. Lymphatic endothelium in health and disease. *Cell Tissue Res*. 2009;335(1):97-108.
3. Petrova TV, Koh GY. Organ-specific lymphatic vasculature: from development to pathophysiology. *J Exp Med*. 2018;215(1):35-49.
4. Breslin JW, Yang Y, Scallan JP, Sweat RS, Adderley SP, Murfee WL. Lymphatic vessel network structure and physiology. *Compr Physiol*. 2018;9(1):207-299.
5. Choi I, Lee S, Hong YK. The new era of the lymphatic system: no longer secondary to the blood vascular system. *Cold Spring Harb Perspect Med*. 2012;2(4):a006445.
6. Rockson SG. Acquired lymphedema: abnormal fluid clearance engenders tissue remodeling. *Lymphat Res Biol*. 2014;12(1):1.
7. Wiig H, Swartz MA. Interstitial fluid and lymph formation and transport: physiological regulation and roles in inflammation and cancer. *Physiol Rev*. 2012;92(3):1005-1060.
8. Olszewski WL. Lymphatics, lymph and lymphoid cells: an integrated immune system. *Eur Surg Res*. 1986;18(3-4):264-270.
9. Rockson SG. Lymphatics: where the circulation meets the immune system. *Lymphat Res Biol*. 2013;11(3):115.
10. Permanyer M, Bosnjak B, Forster R. Dendritic cells, T cells and lymphatics: dialogues in migration and beyond. *Curr Opin Immunol*. 2018;53:173-179.
11. Zhang F, Zarkada G, Han J, et al. Lacteal junction zippering protects against diet-induced obesity. *Science*. 2018;361(6402):599-603.
12. Suh SH, Choe K, Hong SP, et al. Gut microbiota regulates lacteal integrity by inducing VEGF-C in intestinal villus macrophages. *EMBO Rep*. 2019;20(4):e46927.
13. Choe K, Jang JY, Park I, et al. Intravital imaging of intestinal lacteals unveils lipid drainage through contractility. *J Clin Invest*. 2015;125(11):4042-4052.
14. Louveau A, Herz J, Alme MN, et al. CNS lymphatic drainage and neuroinflammation are regulated by meningeal lymphatic vasculature. *Nat Neurosci*. 2018;21(10):1380-1391.
15. Louveau A, Plog BA, Antila S, Alitalo K, Nedergaard M, Kipnis J. Understanding the functions and relationships of the glymphatic system and meningeal lymphatics. *J Clin Invest*. 2017;127(9):3210-3219.
16. Da Mesquita S, Louveau A, Vaccari A, et al. Functional aspects of meningeal lymphatics in ageing and Alzheimer's disease. *Nature*. 2018;560(7717):185-191.
17. Ridner SH. Pathophysiology of lymphedema. *Semin Oncol Nurs*. 2013;29(1):4-11.
18. Noon A, Hunter RJ, Witte MH, et al. Comparative lymphatic, ocular, and metabolic phenotypes of Foxc2 haploinsufficient and aP2-FOXC2 transgenic mice. *Lymphology*. 2006;39(2):84-94.
19. Teerachaisakul M, Ekataksin W, Durongwatana S, Taneepanichskul S. Risk factors for cellulitis in patients with lymphedema: a case-controlled study. *Lymphology*. 2013;46(3):150-156.
20. Kataru RP, Baik JE, Park HJ, et al. Regulation of immune function by the lymphatic system in lymphedema. *Front Immunol*. 2019;10:470.
21. Chakraborty A, Barajas S, Lammoglia GM, et al. Vascular endothelial. Growth factor-D (VEGF-D) overexpression and lymphatic expansion in murine adipose tissue improves metabolism in obesity. *Am J Pathol*. 2019;189(4):924-939.
22. Lee E, Pandey NB, Popel AS. Crosstalk between cancer cells and blood endothelial and lymphatic endothelial cells in tumour and organ microenvironment. *Expert Rev Mol Med*. 2015;17:e3.
23. Lee E, Fertig EJ, Jin K, Sukumar S, Pandey NB, Popel AS. Breast cancer cells condition lymphatic endothelial cells within pre-metastatic niches to promote metastasis. *Nat Commun*. 2014;5:4715.
24. Kataru RP, Ly CL, Shin J, et al. Tumor lymphatic function regulates tumor inflammatory and immunosuppressive microenvironments. *Cancer Immunol Res*. 2019;7(8):1345-1358.
25. Garnier L, Gkoutidi AO, Hugues S. Tumor-associated lymphatic vessel features and immunomodulatory functions. *Front Immunol*. 2019;10:720.
26. Mathieu E, Gupta N, Macdonald RL, Ai J, Yucel YH. In vivo imaging of lymphatic drainage of cerebrospinal fluid in mouse. *Fluids Barriers CNS*. 2013;10(1):35.
27. Laborda E, Santesteban P, Samaniego E. Unusual lymphatic drainage pattern in a patient with lymphedema of lower extremities. *Lymphology*. 2005;38(1):16-17.
28. von der Weid PY, Zawieja DC. Lymphatic smooth muscle: the motor unit of lymph drainage. *Int J Biochem Cell Biol*. 2004;36(7):1147-1153.
29. Liao S, von der Weid PY. Inflammation-induced lymphangiogenesis and lymphatic dysfunction. *Angiogenesis*. 2014;17(2):325-334.
30. Baluk P, Fuxe J, Hashizume H, et al. Functionally specialized junctions between endothelial cells of lymphatic vessels. *J Exp Med*. 2007;204(10):2349-2362.
31. Kawai Y, Kaidoh M, Yokoyama Y, Ohhashi T. Pivotal roles of lymphatic endothelial cell layers in the permeability to hydrophilic substances through collecting lymph vessel walls: effects of inflammatory cytokines. *Lymphat Res Biol*. 2014;12(3):124-135.
32. Foster RS Jr. General anatomy of the lymphatic system. *Surg Oncol Clin N Am*. 1996;5(1):1-13.
33. Choi D, Park E, Jung E, et al. Laminar flow downregulates Notch activity to promote lymphatic sprouting. *J Clin Invest*. 2017;127(4):1225-1240.
34. Danussi C, Del Bel BL, Pivetta E, et al. EMLIN1/alpha9beta1 integrin interaction is crucial in lymphatic valve formation and maintenance. *Mol Cell Biol*. 2013;33(22):4381-4394.
35. Motawe ZY, Abdelmaboud SS, Breslin JW. Involvement of sigma receptor-1 in lymphatic endothelial barrier integrity and bioenergetic regulation. *Lymphat Res Biol*. 2020;19(3):231-239.
36. Murfee WL, Breslin JW. Linking lymphatic function to disease. *J Physiol*. 2020;598(15):3065-3066.
37. Loo CP, Nelson NA, Lane RS, et al. Lymphatic vessels balance viral dissemination and immune activation following cutaneous viral infection. *Cell Rep*. 2017;20(13):3176-3187.
38. Lund AW, Wagner M, Fankhauser M, et al. Lymphatic vessels regulate immune microenvironments in human and murine melanoma. *J Clin Invest*. 2016;126(9):3389-3402.
39. Lee J, Breuer CB, Lee E. Bioengineered in vitro models of leukocyte-vascular interactions. *Biochem Soc Trans*. 2021;49(2):693-704.
40. Kesler CT, Pereira ER, Cui CH, et al. Angiotensin-1 increases permeability of blood vessels and promotes lymphatic dilation. *FASEB J*. 2015;29(9):3668-3677.
41. Modi S, Stanton AW, Mellor RH, Peters AM, Levick JR, Mortimer PS. Regional distribution of epifascial swelling and epifascial lymph drainage rate constants in breast cancer-related lymphedema. *Lymphat Res Biol*. 2005;3(1):3-15.
42. Lutter S, Makinen T. Regulation of lymphatic vasculature by extracellular matrix. *Adv Anat Embryol Cell Biol*. 2013;214:55-65.
43. Dejana E, Orsenigo F, Molendini C, Baluk P, McDonald DM. Organization and signaling of endothelial cell-to-cell junctions in various regions of the blood and lymphatic vascular trees. *Cell Tissue Res*. 2009;335(1):17-25.
44. Triacca V, Guc E, Kilarski WW, Pisano M, Swartz MA. Transcellular pathways in lymphatic endothelial cells regulate changes in solute transport by fluid stress. *Circ Res*. 2017;120(9):1440-1452.
45. Wang Y, Simons M. Flow-regulated lymphatic vasculature development and signaling. *Vasc Cell*. 2014;6:14.
46. Ng CP, Helm CL, Swartz MA. Interstitial flow differentially stimulates blood and lymphatic endothelial cell morphogenesis in vitro. *Microvasc Res*. 2004;68(3):258-264.
47. Herpertz U. Complications in lymphedema. *Z Lymphol*. 1993;17(2):48-53.
48. Rockson SG. Molecular mechanisms in lymphatic function and disease. *Lymphat Res Biol*. 2006;4(3):117.

49. Cueni LN, Detmar M. The lymphatic system in health and disease. *Lymphat Res Biol*. 2008;6(3-4):109-122.
50. Lutter S, Makinen T. Regulation of lymphatic vasculature by extracellular matrix. *Adv Anat Embryol Cell Biol*. 2014;214:55-65.
51. Lutter S, Xie S, Tatin F, Makinen T. Smooth muscle-endothelial cell communication activates Reelin signaling and regulates lymphatic vessel formation. *J Cell Biol*. 2012;197(6):837-849.
52. Altiok E, Ecoiffier T, Sessa R, et al. Integrin alpha-9 mediates lymphatic valve formation in corneal lymphangiogenesis. *Invest Ophthalmol vis Sci*. 2015;56(11):6313-6319.
53. Valdembri D, Serini G. The roles of integrins in cancer. *Fac Rev*. 2021;10:45.
54. Ecker BL, Kaur A, Douglass SM, et al. Age-related changes in HAPLN1 increase lymphatic permeability and affect routes of melanoma metastasis. *Cancer Discov*. 2019;9(1):82-95.
55. Baker BM, Chen CS. Deconstructing the third dimension: how 3D culture microenvironments alter cellular cues. *J Cell Sci*. 2012;125(Pt 13):3015-3024.
56. Kwak TJ, Lee E. Rapid multilayer microfabrication for modeling organotrophic metastasis in breast cancer. *Biofabrication*. 2020;13(1):15002.
57. Kwak TJ, Lee E. In vitro modeling of solid tumor interactions with perfused blood vessels. *Sci Rep*. 2020;10(1):20142.
58. Polacheck WJ, Kutys ML, Tefft JB, Chen CS. Microfabricated blood vessels for modeling the vascular transport barrier. *Nat Protoc*. 2019;14(5):1425-1454.
59. Dixon JB, Greiner ST, Gashev AA, Cote GL, Moore JE, Zawieja DC. Lymph flow, shear stress, and lymphocyte velocity in rat mesenteric prenodal lymphatics. *Microcirculation*. 2006;13(7):597-610.
60. Polacheck WJ, Kutys ML, Yang J, et al. A non-canonical Notch complex regulates adherens junctions and vascular barrier function. *Nature*. 2017;552(7684):258-262.
61. Adamson R, Lenz J, Curry F. Quantitative laser scanning confocal microscopy on single capillaries: permeability measurement. *Microcirculation*. 1994;1(4):251-265.
62. Schindelin J, Arganda-Carreras I, Frise E, et al. Fiji: an open-source platform for biological-image analysis. *Nat Methods*. 2012;9(7):676-682.
63. Schneider CA, Rasband WS, Eliceiri KW. NIH Image to ImageJ: 25 years of image analysis. *Nat Methods*. 2012;9(7):671-675.
64. Acevedo-Acevedo S, Crone WC. Substrate stiffness effect and chromosome missegregation in hPS cells. *J Negat Results Biomed*. 2015;14:22.
65. Raub CB, Putnam AJ, Tromberg BJ, George SC. Predicting bulk mechanical properties of cellularized collagen gels using multiphoton microscopy. *Acta Biomater*. 2010;6(12):4657-4665.
66. Urbich C, Dernbach E, Reissner A, Vasa M, Zeiher AM, Dimmeler S. Shear stress-induced endothelial cell migration involves integrin signaling via the fibronectin receptor subunits alpha(5) and beta(1). *Arterioscler Thromb Vasc Biol*. 2002;22(1):69-75.
67. Hofer U, Syfrig J, Chiquet-Ehrismann R. Identification and characterization of a dimeric chicken fibronectin receptor. Subunit-specific monoclonal antibodies to the putative chicken alpha 5 beta 1 integrin. *J Biol Chem*. 1990;265(24):14561-14565.
68. Turner CJ, Badu-Nkansah K, Hynes RO. Endothelium-derived fibronectin regulates neonatal vascular morphogenesis in an autocrine fashion. *Angiogenesis*. 2017;20(4):519-531.
69. Henderson AR, Choi H, Lee E. Blood and lymphatic vasculatures on-chip platforms and their applications for organ-specific in vitro modeling. *Micromachines (Basel)*. 2020;11(2):147.
70. Lee E, Song HG, Chen CS. Biomimetic on-a-chip platforms for studying cancer metastasis. *Curr Opin Chem Eng*. 2016;11:20-27.
71. Perel P, Roberts I, Sena E, et al. Comparison of treatment effects between animal experiments and clinical trials: systematic review. *BMJ*. 2007;334(7586):197.
72. Selimovic S, Dokmeci MR, Khademhosseini A. Organs-on-a-chip for drug discovery. *Curr Opin Pharmacol*. 2013;13(5):829-833.
73. Thomas SN, Vokali E, Lund AW, Hubbell JA, Swartz MA. Targeting the tumor-draining lymph node with adjuvanted nanoparticles reshapes the anti-tumor immune response. *Biomaterials*. 2014;35(2):814-824.
74. Hooks JST, Clement CC, Nguyen HD, Santambrogio L, Dixon JB. In vitro model reveals a role for mechanical stretch in the remodeling response of lymphatic muscle cells. *Microcirculation*. 2019;26(1):e12512.
75. Gibot L, Galbraith T, Bourland J, Rogic A, Skobe M, Auger FA. Tissue-engineered 3D human lymphatic microvascular network for in vitro studies of lymphangiogenesis. *Nat Protoc*. 2017;12(5):1077-1088.
76. Gibot L, Galbraith T, Kloos B, et al. Cell-based approach for 3D reconstruction of lymphatic capillaries in vitro reveals distinct functions of HGF and VEGF-C in lymphangiogenesis. *Biomaterials*. 2016;78:129-139.
77. Rogic A, Auger F, Skobe M. Isolation of human skin lymphatic endothelial cells and 3D reconstruction of the lymphatic vasculature in vitro. *Methods Mol Biol*. 2018;1846:279-290.
78. Morgan MM, Schuler LA, Ciciliano JC, Johnson BP, Alarid ET, Beebe DJ. Modeling chemical effects on breast cancer: the importance of the microenvironment in vitro. *Integr Biol (Camb)*. 2020;12(2):21-33.
79. Thompson RL, Margolis EA, Ryan TJ, et al. Design principles for lymphatic drainage of fluid and solutes from collagen scaffolds. *J Biomed Mater Res A*. 2018;106(1):106-114.
80. Wong KH, Truslow JG, Khankhel AH, Chan KL, Tien J. Artificial lymphatic drainage systems for vascularized microfluidic scaffolds. *J Biomed Mater Res A*. 2013;101(8):2181-2190.
81. Scallan JP, Davis MJ, Huxley VH. Permeability and contractile responses of collecting lymphatic vessels elicited by atrial and brain natriuretic peptides. *J Physiol*. 2013;591(20):5071-5081.
82. Scallan JP, Huxley VH. In vivo determination of collecting lymphatic vessel permeability to albumin: a role for lymphatics in exchange. *J Physiol*. 2010;588(Pt 1):243-254.
83. Price GM, Chrobak KM, Tien J. Effect of cyclic AMP on barrier function of human lymphatic microvascular tubes. *Microvasc Res*. 2008;76(1):46-51.

SUPPORTING INFORMATION

Additional supporting information may be found in the online version of the article at the publisher's website.

How to cite this article: Henderson AR, Ilan IS, Lee E. A bioengineered lymphatic vessel model for studying lymphatic endothelial cell-cell junction and barrier function. *Microcirculation*. 2021;00:e12730. doi:[10.1111/micc.12730](https://doi.org/10.1111/micc.12730)